LANGMUIR



New Concepts at the Interface: Novel Viewpoints and Interpretations, Theory and Computations

# A General Computational Methodology for Modelling Electrohydrodynamic Flows: Prediction and Optimisation Capability for the Generation of Bubbles and Fibres

Babatunde Aramide, Anjana Kothandaraman, Mohan Edirisinghe, Suwan N. Jayasinghe, and Yiannis Ventikos

*Langmuir*, **Just Accepted Manuscript** • DOI: 10.1021/acs.langmuir.8b03763 • Publication Date (Web): 20 Mar 2019

# A General Computational Methodology for Modelling Electrohydrodynamic Flows: Prediction and Optimisation Capability for the Generation of Bubbles and Fibres

Babatunde Aramide[1], Anjana Kothandaraman[1*],
Mohan Edirisinghe[1], Suwan N. Jayasinghe[1], Yiannis Ventikos[1+]
[1] Department of Mechanical Engineering, University College London, London, WC1E 7JE, UK.
* Currently: Department of Mechanical Engineering, University of Birmingham, Birmingham B15 2TT, UK.
[+] Correspondence: y.ventikos@ucl.ac.uk

## ABSTRACT

The application of an electric field on a fluid in motion gives rise to unique features and flow manipulation capabilities. Technologies ranging from bubble formation, droplet generation, fibre spinning, and many others are predicated on this type of flows, often referred to as Electrohydrodynamics (EHD). In this paper, we present a numerical methodology that allows for the modelling of such processes in a generalised way. The method can account for the pre-mixing of various liquid species, the injection of gases in the mixture and the interaction of such complex multi-phase flow with an electric field, static or AC. The domain in which these processes take place can be of arbitrary geometric complexity, allowing for design and optimisation of complex EHD devices. Our study looks at the critical phases of some of these processes and emphasizes the strong coupling of fluid mechanics and electric fields and the influence of the electric field on fluid flow and vice versa.

The conservation of mass and momentum, with appropriate additional force terms coming from the presence of the electric field, and the electrostatic equations are coupled together and solved using the Finite Volume method. The Volume of Fluid (VoF) technique is used to track free surfaces dynamically. The solution procedure iteratively computes electric body and surface forces and then includes those into the Navier-Stokes equation to predict the velocity field and other fluid parameters. No initial shape is assumed for the fluid(s) and charge distributions.

The methodology presented handles two-dimensional, axisymmetric and full three-dimensional cases, of arbitrary geometric complexity, allowing for mixing and/or microfluidic configurations of high levels of realism. We highlight the capability of the method by demonstrating cases like the formation of a Taylor cone, microfluidic bubble generation, jet evolution and droplet break-up. Results agree well with both existing experimental and computational reports.

## 1. INTRODUCTION TO EHD

Electrohydrodynamics (EHD) involves studying the fluid motion induced or affected by electrical fields [1]; in other words, it deals with the interaction of fluid flow and electric fields [2]. It is an interdisciplinary field involving branches such as hydrodynamics, thermophysics, electrochemistry and electrostatics [3]. EHD transport phenomena are fundamental to a range of applications in engineering, including electrospray ionization, electrospinning, electrostatic printing, electrokinetic assays etc. [4]. The electrostatic field generated exerts additional electromechanical forces in the normal and tangential direction of the liquid [5].

A hallmark of EHD-related flow features is the formation of the Taylor cone.

Figure 1 shows the schematic of this formation [6]. The Coulombic forces induced by the electric field and the electrostatic repulsive forces due to the surface charges are the two main electrostatic forces that a liquid – say a polymer – volume experiences [7] to form this cone. Prior to the application of the high voltage to the spinneret, the tip of the polymer droplet is held by its own surface tension [8].

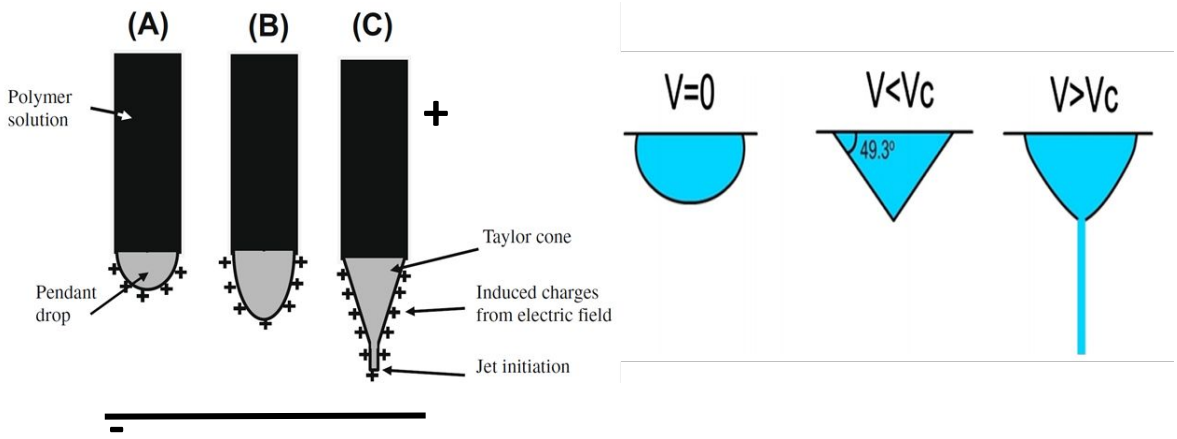


Figure 1- Taylor cone formation and jet initiation, modified from [9,10]

As the electric field, V attains a critical value, $V_c$ the electrostatic forces finally overcome the surface tension in the polymeric solution and this commences the ejection of the polymer jet from the tip of the Taylor cone [8].

Various EHD flow patterns emerge as the electric field strength and the liquid flow rate are varied. A possible representation by Collins et al [11], is shown schematically in Figure 2. Depending on the intended application, the operational map parameters are chosen to aid the needed flow pattern. The jetting mode, cone-jet mode and others as shown in Figure 2 have found application in areas like electrospray, electrospinning, ink-jet printing. [12–14].

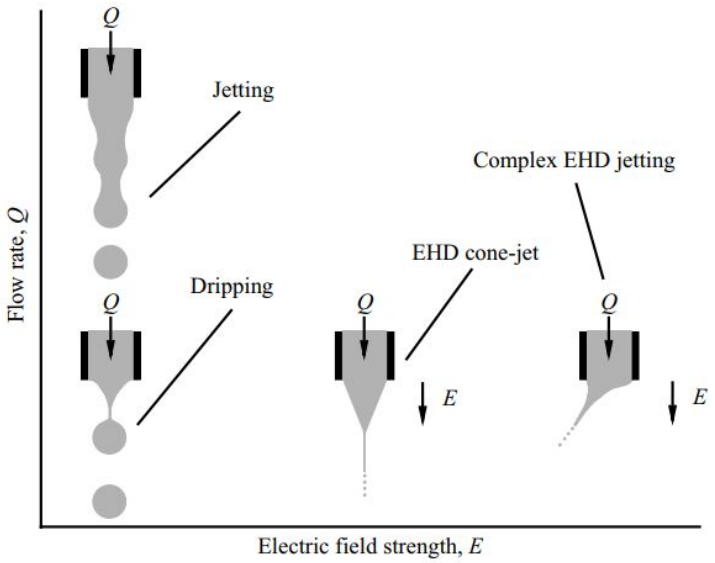


Figure 2- Phase diagram depicting flow transitions that occur as flow rate and/or electric field vary [11]

Several studies have been pursued to provide insight into the cone-Jet mode. Worthy of mention are the foundational works by Zeleny [15] and Taylor [16] where the phenomenon of how water drops disintegrate under the influence of an electric field has been highlighted. They also studied the stresses acting on a spherical fluid volume – a droplet – due to the presence of an electric field. Ajayi [17] also noted the boundary conditions to be satisfied at the surface of a deformed drop. Taylor [18] further described the behaviour of stability of electrified jets. Melcher and Taylor [19] then extended this basic understanding to further expand the scope of EHD to explore the role of interfacial shear stresses acting on the liquid-air interface. A robust mathematical formulation of the work by Melcher and Taylor has been shown in [2].

Regarding computational modelling, Hartman et al [20,21] performed numerical simulations on Electrohydrodynamic Atomization (EHDA) to predict the shape of the liquid cone and resulting jet, they also were able to highlight the characteristic pattern of the electric fields- both in and outside the liquid cone as well as the surface charge density of the jets. These models did not involve capturing the jet breakup mode of the process. The cone-jet mode has also been predicted by Yan et al [22] by solving the axisymmetric equations for EHD. Their model was able to calculate the cone-jet shape and velocity field with the liquid meniscus. Notably, the work of Lastow and Balachandran [23] on EHDA was markedly successful, since they were able to predict droplet size and diameter in very good comparison with experimental data.

Another particularly important feature produced from EHDA multi-phase interactions is microbubble generation, of particular interest to this study. Controlled production of microbubbles is of growing interest in various fields of applications like tissue engineering, drug delivery, water management, food engineering etc. [24]. Controlled generation and breaking of liquid films result in the development of bubbles. Microbubble and droplet formation is mainly realised via three mechanisms- depending on the geometry of the set-up and the nature of the flow field break-up: a) Cross Flow, b) Flow focusing and c) Co-flowing techniques [25]. Some jetting configurations have been depicted in Figure 3. For the purposes of this study, we have chosen to demonstrate the methodology developed in a Cross Flow configuration, also known as a T-junction, with no loss of generality regarding the applicability of the method.

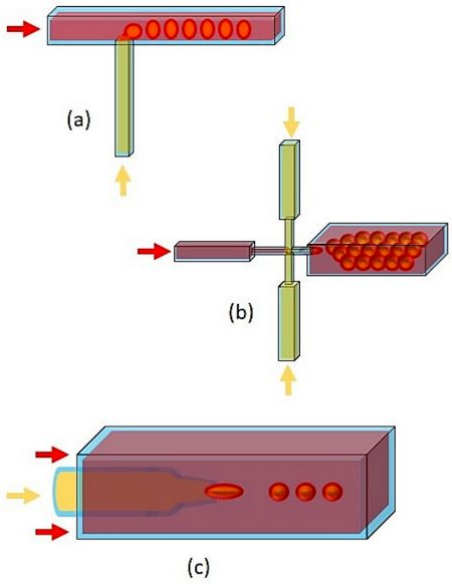


Figure 3- Droplet generation by microfluidic systems:
(a) T-junction; (b) Flow-focusing; (c) Co-flow (glass capillary) [26]

The phenomena described in these works are critical in grasping the physics behind electrified flows, with the primary objectives aimed at understanding the formation of microbubbles, cone-jets and droplets. These works also established the dual-coupling nature of the EHD problem, i.e. the hydrodynamic and the electrostatic interactions. Our model, based on the above considerations, presents a generalised computational method for handling all such phenomena in an integrative manner.

## 2. GOVERNING EQUATIONS AND NUMERICAL METHODS

### 2.1 Interface and Shear Stresses in EHD

We shall utilise the Taylor cone geometry to exemplify and cast the equations at play – exactly analogous considerations apply in other cases; droplets and bubbles; where interfaces are present. At the interface of two phases – liquid and gas – there is an accumulation of electrodynamic charges and a coupling between the hydrodynamic forces between the two fluids [27]. Here the viscous flow balances the tangential electric stress and the normal component of the electric stress is counterbalanced by the surface tension of the solution (assuming continuity of pressure). Figure 4 shows a schematic representation of the forces acting on a liquid jet in the presence of an electric field.

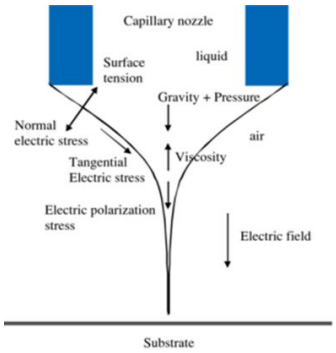


Figure 4- Forces acting on a liquid jet in the presence of an electric field[20]

To understand the role of the electrical field in the EHD flow, this section will discuss the three additional stresses acting at the interface of the jet; analysing their sources and the effects of their components. Table 1 shows a summary of the electrostatic forces on a jet under the influence of an electric field, highlighting the sources, effects and the mathematical expressions describing these forces in terms of the applied electric field, electric charge and permittivity of the medium.

Table 1- Electric forces on electrified interfaces

| COMPONENT | SOURCE | EFFECT | EXPRESSION |
|---|---|---|---|
| Polarization force | Permittivity gradient at the liquid-gas interface | Resist the local constriction of the electric field | $\frac{1}{2}E^2\nabla\varepsilon$ |
| Tangential electric forces | Free surface charge | • Provides longitudinal stretching by accelerating the jet flow<br>• Promotes electrical whipping mode | |
| Coulombic/Normal electric forces | Self-repulsion of the free-surface charges. | • Balances and reduces the effect of surface tension<br>• Promotes electrical whipping mode | $qE$ |

There is a large jump in the electric field across the interface/free surface. This jump is responsible for both the tangential and normal electric stresses. In the case of a cone/jet configuration, the normal stress is attributed to maintaining the conical shape of the liquid, while the tangential component accelerates the liquid in the direction of the resulting jet [28].

For leaky-dielectrics, the coupling of the hydrodynamics and electric fields occurs only at the liquid-air boundaries/interface- where electric stresses that are different from those of perfect conductors and dielectrics are developed by charges carried to the surface by conduction [2]. To further understand the role and direction of action of the forces, Chen [29] described the bisect rule which allows to graphically identify the direction of the electric stresses given that the direction of applied electric field is known. According to Panofsky and Philips [30], Figure 5, the Bisect Rule states that: "For a surface $dS$, in a dielectric medium with permittivity of $\varepsilon$, the electric field $(E)$ bisects the angle between the normal to the surface $(n)$ and the resultant force $(F^e)$ whose magnitude is $F^e dS = \frac{1}{2}\varepsilon E^2 dS$ ."

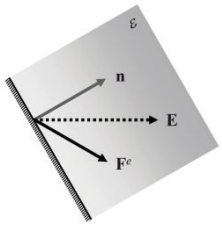


Figure 5- The Bisect Rule [29]

Figure 6 shows the different applications of this rule for various liquids and shapes under the action of an electric field.

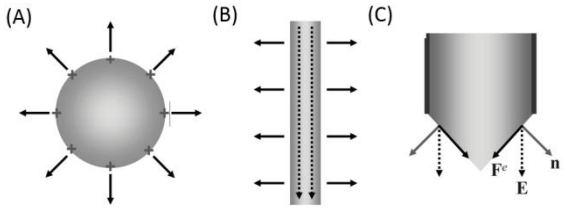


Figure 6- Applications of Bisect Rule- (A) Perfect conductor; (B) Perfect Dielectric; (C) Leaky-Dielectric [29]

For a perfect conductor (with zero permittivity), as shown in Figure 6 (A), the Coulombic force which is due to free charges acts along the electric field which is perpendicular to the free surface. Figure 6 (B) depicts a perfect dielectric (insulator, with zero conductivity), where the polarization force acts along the electric field and is perpendicular to the interface. The third scenario is the case of a leaky-dielectric (i.e. non zero permittivity and conductivity), tangential stress develops on the cone interface, where the electric field is at 45° to the normal, as shown in Figure 6 (C) [29,30].

Similarly, the electric stress is normal to and changes with the interface profile alongside the surface tension (which balances the electric stress) in the case of perfect conductors and perfect dielectrics. On the other hand, for leaky-dielectrics the interfacial charges alter the electric field, thereby giving rise to the development of a viscous flow to balance the resultant force due to the tangential components at the interface [28]. Summarily, the electric stress acts perpendicularly to the interface for both the perfect conductor and dielectric. But for the leaky-dielectric, the accumulated free charges on the interface may modify the field drastically. A resultant viscous flow (which is stretched and accelerated) then develops, to provide forces (shear stresses) that counter-balances the action of the tangential component of the field.

### 2.2 General Momentum Balance Equation for the Dielectric Fluid.

The differential equations describing EHD arise from the combination of equations describing the conservation of mass and momentum for a continuum phase (or multiple continuum phases), and Maxwell's equations [2]. The Maxwell stress tensor couples the electrostatic and hydrodynamics equations, hence it is essential in the formulation of EHD problems [29]. The forces acting on the system account for the liquid deformation and charge distribution [31]. The leaky dielectric model assumes that the fluid medium acts as an ohmic conductor i.e. the conductivity is constant. This assumption is valid for fluids with more or less constant properties (for example constant density, i.e., an immiscible phase and incompressible flow). Therefore, it is the combination of a Charge Transport Model and the Navier-Stokes equations that form the leaky dielectric EHD model [32].

#### 2.2.1 Continuity Equation

$$\nabla . \vec{u} = 0 \qquad (2)$$

where $\vec{u}$ is the flow velocity field.

#### 2.2.2 Momentum Conservation Equation

The modified Navier-Stokes equation for an EHD flow is given as:

$$\rho\frac{\partial \vec{u}}{\partial t}+\rho\vec{u}.\nabla\vec{u}=-\nabla p+\mu\nabla^2\vec{u}+\rho g+F_e \quad (3)$$

where $\rho$ is the fluid density, $p$ is the hydrostatic pressure, $\mu$ is the viscosity, $g$ is the gravitational force and $F_e$ is the extra electromechanical term that arises due to the applied electric field, it is also called the Maxwell Tensor.

### 2.2.3 Electric Field Equations

The electromechanical force can be expressed as

$$F_e=qE-\frac{E^2}{2}\nabla\varepsilon+\nabla\left[\rho\frac{E^2}{2}\left(\frac{\partial\varepsilon}{\partial\rho}\right)\right] \quad (4)$$

where $E$ is the electric field, $\varepsilon$ is the permittivity if the medium and $q$ is the free charge density of the applied electric field. The first term in equation (4) is referred to as the Coulombic force, the last two terms are jointly referred to as polarization forces (the former is known as dielectric force and the latter electrostrictive force). The electrostriction force density is associated with the volumetric change in the medium, which is usually neglected since the medium we are dealing with is incompressible and the permittivity is constant [23]. The electrical force is given as the sum of Coulombic Force and Polarization Stress. Both of these act at the interface since the electric charges accumulate at the air-liquid interface. [33].

The generalised EHD equation is therefore expressed as:

$$\rho\frac{\partial \vec{u}}{\partial t}+\rho\vec{u}.\nabla\vec{u}=-\nabla p+\mu\nabla^2\vec{u}+\rho g+qE-\frac{E^2}{2}\nabla\varepsilon+\nabla\left[\rho\frac{E^2}{2}\left(\frac{\partial\varepsilon}{\partial\rho}\right)\right] \quad (5)$$

### 2.2.4 The Ohmic Model

The Ohmic model provides an approximation for the EHD phenomena [19,29]. In this model, the EHD is approximated as being electroquasistatic and the effect of the magnetic field is negligible and can be ignored and it is thus solenoidal and described by:

$$\nabla\times E=0 \quad (6)$$

The electric field, $E$, follows Gauss's law, which is approximated as

$$\nabla\cdot\varepsilon E=q \quad (7)$$

where $\varepsilon$ is the permittivity of the medium and $q$ is the free charge density of the applied electric field.

In a leaky-dielectric model, an Ohmic constitutive law of current is assumed [19], with the diffusive current ignored.

$$i=i_c+i_o=qv+\sigma E \quad (8)$$

where $\dot{I}_c$ is the convective current and $\dot{I}_0$ is the ohmic current.

The charge conservation equation relates the free charge density to current, $(i)$ by:

$$\frac{\partial q}{\partial t} + \nabla \cdot i = 0 \tag{9}$$

Therefore,

$$\frac{\partial q}{\partial t} + \nabla \cdot qv + \nabla \cdot \sigma E = 0 \tag{10}$$

The expression in (10) describes the charge conservation in the ohmic region, where the electric field, $E = -\nabla \phi$ . $\phi$ is the electric field potential of the medium.

The Ohmic model includes both the conductivity and free density charge conservation equation. The two most important assumptions in this model are that the diffusive current and the instantaneous charge relaxation are negligible. These assumptions are relevant for an EHD process where the time scale and length scale of interest are typically larger than $1ms$ and $1\mu m$ respectively. Generally, the ohmic law is not applicable in the case of an electric double layer where the length of interest of the charged layer is less than $1\mu m$ .

### 2.2.5 Computational Method

For the models in the research work herein, the Finite Volume Method (FVM) technique is adopted to discretize the differential equations into algebraic equations: FMV was chosen because of its conservative properties. A segregated solution method is employed where each momentum equation is solved separately, under an assumed pressure field – subsequently, the pressure is updated using a pressure correction algorithm. Each variable, therefore, results in a separate algebraic system, which is solved sequentially and repeatedly until convergence is achieved.

To solve the coupled EHD equations, a technique similar to that used in [23] was expanded, where to solve the leaky dielectric equation, the potential field, $\phi$ was solved to obtain the electric body force. Afterwards, the Navier-Stokes equations were solved to obtain the velocity field and the pressure and velocity were corrected using the SIMPLEC pressure correction method [34]. After obtaining the corrected values of the flow field, the physical properties are redistributed to determine the volume of fluid fractions of the two phases. The VoF method is used in combination with a Piecewise Linear Interface Calculation (PLIC) to capture the evolution interface [35]. All these elements are iterated within each time step until residuals drop below a predefined threshold, to declare converge. All interpolations and finite difference terms within this framework have been computed using a central scheme, yielding, therefore, second-order accuracy spatially. Similarly, a Crank-Nicholson scheme has been used for the temporal discretization, resulting in second-order accuracy in time marching as well [36].

### 2.2.6 The Volume of Fluid Method

Free surfaces connote the interface/boundary of fluid-fluid flow, the fluids usually with a large density difference of approximately 1000:1. This difference usually occurs in a gas-liquid interface. It is from this variation in destiny magnitude that the term 'free' comes. The solution of a free surface flow problem involves finding the free surface location and the flow field bounded by it [6].

Free-surface problems can be categorised into two classes: first are problems in which the solution depends only weakly on the shape of the free surface e.g. most problems involving fluids with negligible surface tension; the second are those problems in which surface tension is a dominant influence [37]. This work falls into the second category.

Various methods have been used to solve free surface problems depending on the scheme used to form the discretisation of the spatial domain and the surface boundary including Boundary-Element methods, Finite-Difference methods (like Marker-and-cell, Volume of Fluid, Level Set and Phase Field) and the finite element methods (e.g. fixed-connectivity meshes and unstructured meshes) [37]. The VOF method is the technique adopted in this work.

The basic idea of the VOF, developed by Hirt and Nichols [38] was to introduce a fraction $F$ assigned to each cell, representing the portion that is occupied by the liquid phase. Descriptively,

$$\mathrm{F(x,y,z,t)}=\begin{cases}0 \text{ the gas cell}\\ 1 \text{ the liquid cell}\\ 0<\mathrm{F}<1 \text{ two phase cell/free surface interface}\end{cases} \tag{11}$$

The fraction $F$ fulfils the kinematic equation:

$$\frac{\partial F}{\partial t}+u\frac{\partial F}{\partial x}+v\frac{\partial F}{\partial y}+w\frac{\partial F}{\partial z}=0 \tag{12}$$

This volume fraction $F$ captured by this additional differential equation is evolved in time to track the relative mixture of the two fluids within the domain, expressed as:

$$F=\frac{F_2}{F_{1-2}=F_1+F_2} \tag{13}$$

The subscripts represent the volumes of fluid 1 and fluid 2, where *F* assumes values between zero and 1 inclusive. The interface shape is reconstructed by interpolation to determine the isosurface corresponding to a value of $F=0.5$. Subsequently, the PLIC surface reconstruction technique is interpolated and creates a smooth surface between the two fluids, based on the above fraction computation. This surface is then used to calculate and incorporate effects of surface tension as additional source terms in the momentum equations. For this work, second-order PLIC is used for surface reconstruction [39]. Here, the liquid-gas interface is assumed to take a planar surface and is subsequently allowed to take any orientation with the cell, this interface hence will generally take the shape of the arbitrary polygonal face.

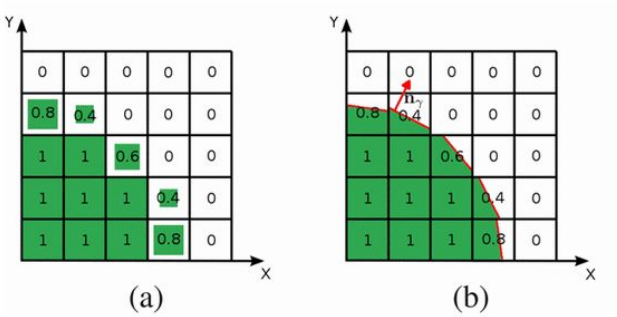


Figure 7- VoF method with PLIC. (a) Distribution of Fluid 2. (b) PLIC reconstruction of the interface [40]

Figure 7 illustrates the PLIC technique for VoF, which tracks the multiphase flow of the advection of the material distribution. Note that higher order PLIC supports the inclusion of surface tension in the solver, therefore it is preferred.

To account for the challenging nature of this multiphysics problem, an automatic time stepping scheme has been used for the computations, with the minimum time step set at $1.0\times10^{-9}s$ and a target CFL of $0.1$.

### 2.3 Meshing

The method is capable of handling 2D, axisymmetric and 3D geometries if appropriate meshing can be constructed. As an example, we can mention that for an axisymmetric model with a charged needle, generating fibres, approximately 50-100K cells - all with structured conforming cells in this case - were used and shown to lead to grid independent results. An illustration of this mesh topology is shown as an example in Figure 8.

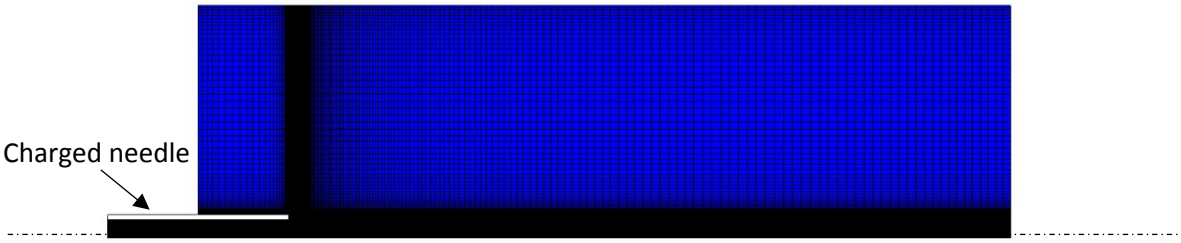


Figure 8- Example of an Axisymmetric Finite Volume Mesh Model

Three-dimensional computations necessitate meshes of approximate 3-7M elements to obtain solutions of similar resolution and mesh independence characteristics.

The modelling components discussed have been implemented within the CFD-ACE+ platform, (ESI Group, Paris, France).

## 3. Results and Discussion

In this section, we demonstrate the methodology by applying it to a series of EHD flows.

### 3.1 Taylor Cone-Jet Formation

This is a base case that forms a common platform for comparisons and for establishing that the balance of viscous, surface tension, inertial, pressure and electrostatic forces indeed accounts for all phenomena in a realistic manner.

### 3.1.1 Fluid Flow Characteristics

No initial assumptions were made for the charge distribution or liquid shape. The effect of the electric field on the liquid distribution, velocity magnitude, charge distribution and electric potential distribution are discussed in the following sections. Several simulations were carried out at various combinations of flow rates and electric voltages to parametrise and explore the conditions affecting this flow.

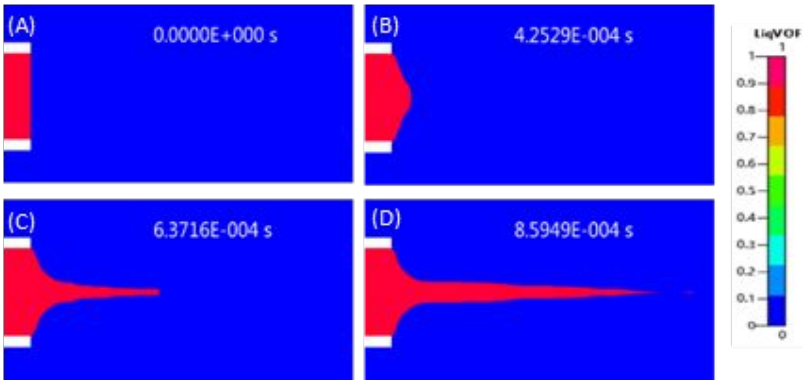


Figure 9- VoF flow distribution at 10kV and inlet velocity of 0.1m/s. (A) t = 0s, (B) t = 42.5ms, (C) 63.7ms and (D) 85.9ms

Under the influence of an applied voltage of magnitude 10kV, the liquid experiences a 4-staged transformation from the initial liquid deformation to the Taylor cone formation to the jetting mode and finally a droplet breakup phase. Initially, the liquid-air interface is flat and as the flow advances, it is deformed due to the interaction of the hydrodynamic and electric forces. The surface tension in the fluid is gradually being overcome by the dielectric force.

After the electric field is applied, the drop liquid deforms into a spherical shape due to EHD liquid flows induced by the charge build-up on the drop surface. Right after the electric field polarity is inverted, the drop rapidly deforms and becomes conical and the first jet was seen to emerge after about 86 milliseconds (as seen in Figure 9).

### 3.1.2 Charge distribution and electric potential distribution

Under the influence of an applied electric field, free charges accumulate at the interface, which induces droplet deformation and EHD flows inside and outside the needle. As expected for a dielectric fluid, the electric charges were mainly localized at the surface of the secondary fluid and very low charge/zero charge density was observed in the bulk of the fluid and of low magnitude in the air. Figure 10 shows the electric field distribution after 47.5 milliseconds when an electric potential of 10kV is applied on the walls of the needle. The Electric field and Electric Potential distribution were shown to evolve, as expected, as the fluid flow advances.

The electric field accounts for both the tangential and normal electric stresses. While the former maintains the conical shape, the latter accelerates the liquid in the direction of the jet.

The applied electric potential induces surface charges on the periphery and not inside the bulk of the fluid jet, and this phenomenon can be seen in the electric field distribution, Figure 10.

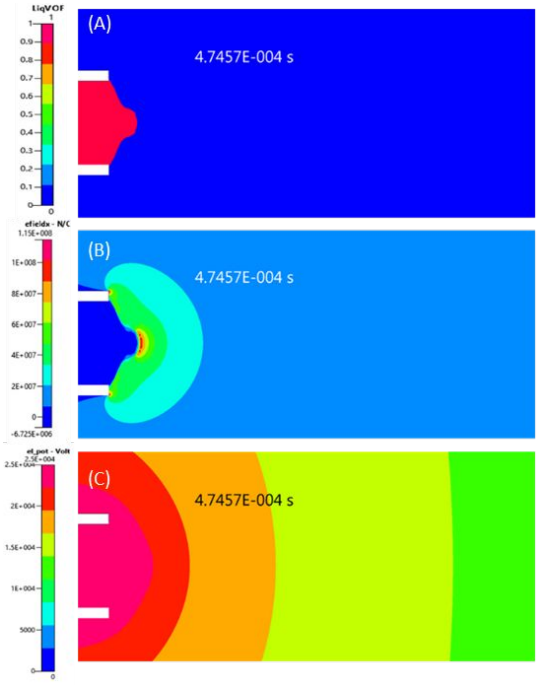


Figure 10- (A) VoF distributions, (B) Electric Field and (C) Electric Potential, at 47.5ms.

Taylor and Melcher [18,19] argued that the surface charges were adequately balanced by the surface tension of the bulk so that a dynamically stable condition is achieved. They noted that the consequence of this interaction is an elongated shape of the fluid volume. This distortion results in the formation of the well-established Taylor cone. The size of this cone is affected by parameters including fluid properties, electric potential and flow rate of the fluid [5,12,41] the effects of which can be evaluated in detail quantitatively in the next phase of this work.

The results obtained to investigate the fluid front interaction with the dynamic electric field also showed good agreement with the work of Sarkar et al [27]. This is a feature that is extremely difficult to visualise experimentally. Figure 11 shows a sample of such results from the present study.

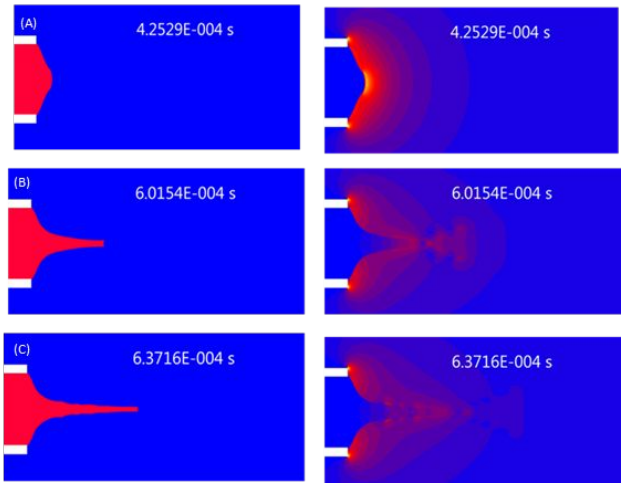


Figure 11- Fluid fonts (left pane) and electric field magnitudes (right pane) at equivalent time steps, showing the interaction of the two flow characteristics. (A) t = 42.5s, (B) t = 60.2ms and (C) 63.7ms

This result implies that the electromagnetic properties (like fluid permittivity, permeability and conductivity) of the fluid can be used to control the fluid front and flow patterns and therefore the EHD cone-jetting mode and other EHD features.

### 3.1.3 Development of Taylor Cone, Jet and Droplet

The droplet development stages are as shown in Figure 12, with a first droplet emerging at about 86 milliseconds when an electric potential of $10kV$ is applied on the wall of the needle at an inlet velocity of $0.1m/s$. See supplementary material 1 for the movie of this jet development.

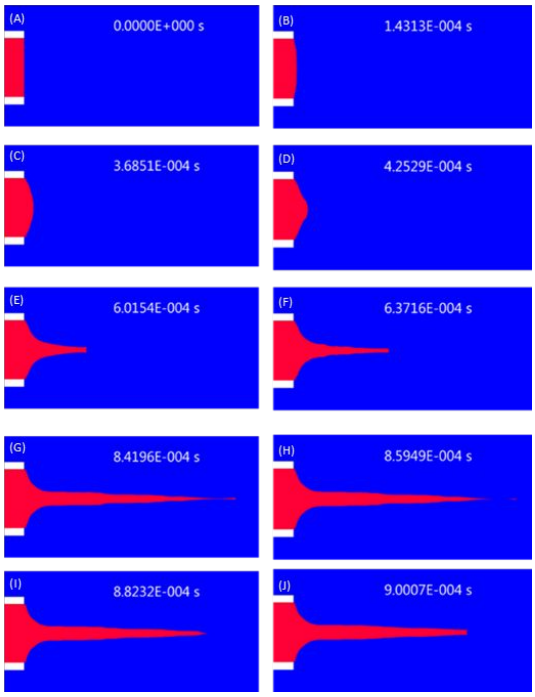


Figure 12- Jet development, showing flow characteristics at various time steps.(A) t = 0s, (B) t = 14.3ms, (C) 36.9ms, (D) 42.5ms, (E) 60.2ms, (F) 63.7ms, fully developed Taylor cone (G) 84.2ms, shortly before the jet break-up occurs (H) 85.9ms, where the jet breaks up (I) 88.2ms and (J) 90.0ms, the jet retracts back into the capillary and the next cycle of jetting begins.

A similar trend was observed in the work of Wu et al [33] as shown in Figure 13 where a dipping mode was predicted at a lower voltage of 900V and a jet break-up mode was predicted at a higher voltage of 1400V. This further strengthens the assertion that the flow transition obtained in an EHD process is dependent on the selected operational map. This implies the model is capable of predicting the flow characteristics from a set of flow parameters.

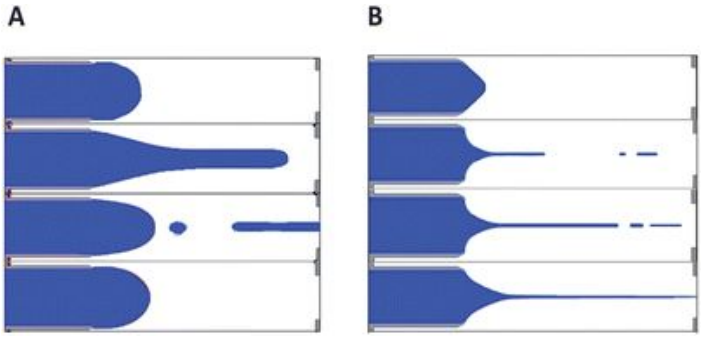


Figure 13- (A) Dipping mode and (B) Jet-Breakup mode at various time steps [33]

### 3.2 Bubble Generation

We further demonstrate the capacity of the method to account for complex EHD flows by simulating the formation of microbubbles from the application of a DC current or a combination of AC and DC electric field in a T-junction. This aspect of the work presents a novel set-up where an alternating current (AC) has been superimposed onto a direct current (DC) field. This enabled us to take advantage of unique characteristics of the AC to control the bubble formation, size and alignment [42]. In Figure 14 the horizontal conduit brings in nitrogen gas, whereas a polymer solution (50% wt. Glycerol + 1% wt. Polyethylene glycol-40-stearate) is injected by the vertical pipe. Figure 14 shows the different development of microbubbles under varying conditions.

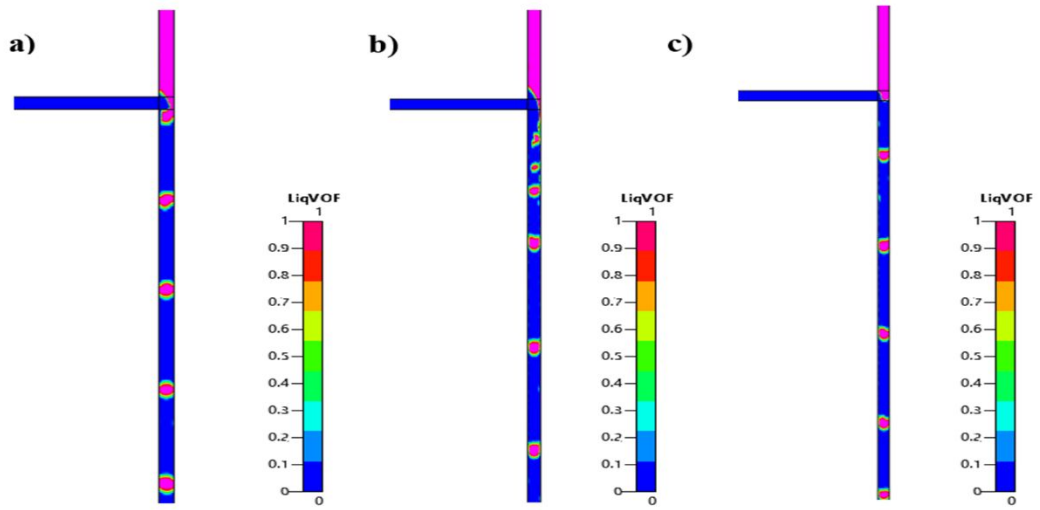


Figure 14- Microbubble formation in the T-junction (a) without an electric field; (b) DC electric field of 6 kV DC; and (c) AC onto DC of 2kVP–P, 6 kV, 2 kHz [42].

The capacity of this methodology to be used as a design tool for EHD processes is illustrated in this example: in Figure 14, we show how the application of an oscillating electric field can be used for the reduction of the size of the produced bubbles- a desired effect in many applications. Without the application of the electric field, the gas enters the main channel and breaks off into bubbles, travelling downstream. When a DC field was applied, smaller bubbles are observed. Further to this, at the point where the bubbles detach from the mainstream, the diameter of the pinch point reduces comparably to the case without the electric field. When an AC field is superimposed on the DC field, even smaller and well-organised bubbles are observed [42].

The model also provides insights to the velocity field around a bubble in microchannels. Without the application of the electric field, the velocity vector distributions display slight perturbations as the bubble traverses along the outlet channel and forming microbubbles of 115 $\mu m$. Similar results were observed in Figure 15b upon application of a DC electric field, where the bubble diameter was recorded to be 108 $\mu m$.

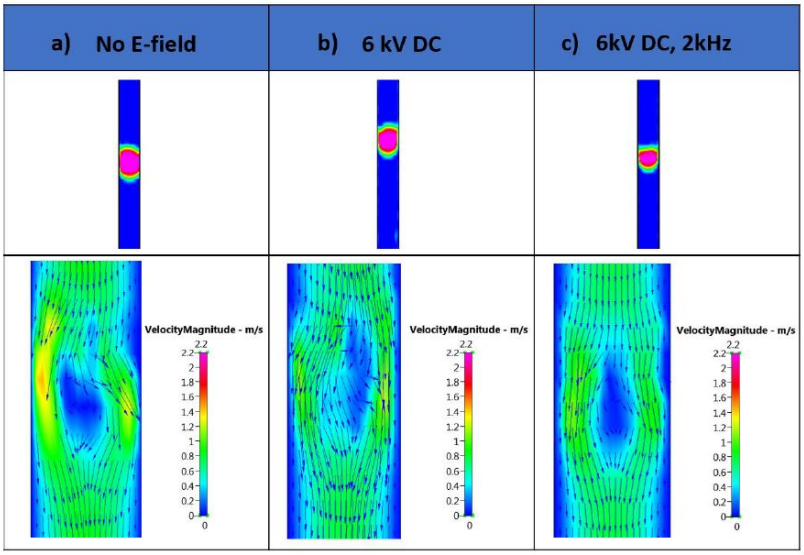


Figure 15- Velocity magnitude vector plots of the microbubble with a) no electric field b) applied DC field of 6KV, and c) applied AC field of 6KV at 2KHz

On the other hand, in the presence of a superimposed field, there is a uniform velocity field distribution along the bubble (Figure 15c) which contributes to the controlled detachment of the emerging microbubble. Increasing the frequency from 0–5$kHz$ results in the decrease in microbubble diameter from 115 $\mu m$ to 60 $\mu m$. Utilising the same parameters, the experimental results resulted in a decrease in microbubble diameter from 111±5.26 $\mu m$ to 31±2.08 $\mu m$. This is summarized in Figure 16.

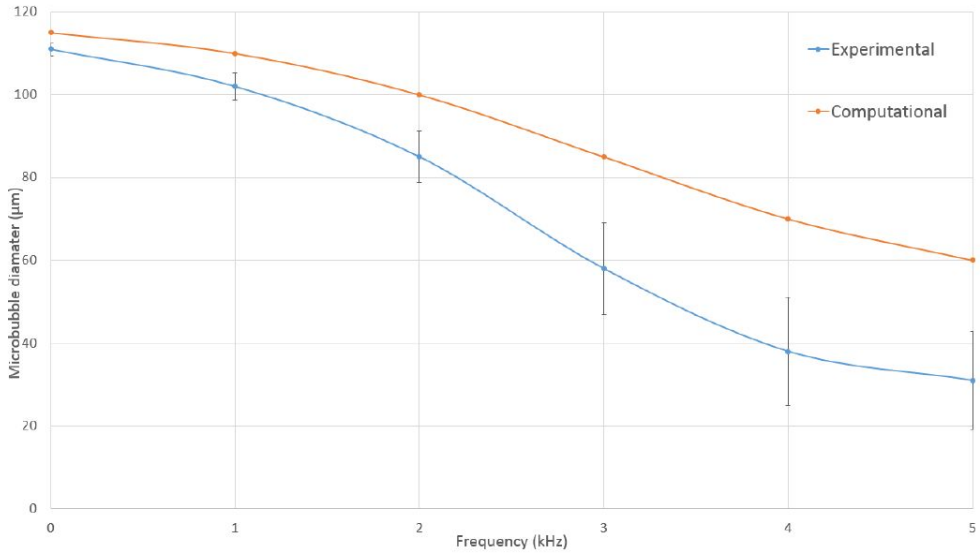


Figure 16- Comparison of microbubble diameter at frequencies 0-5 kHz obtained experimentally and computationally

### 3.3 Droplet Formation

As the last example, we present the development of droplet jetting, achieved at higher flow rates, as summarised by Collins et al [11].

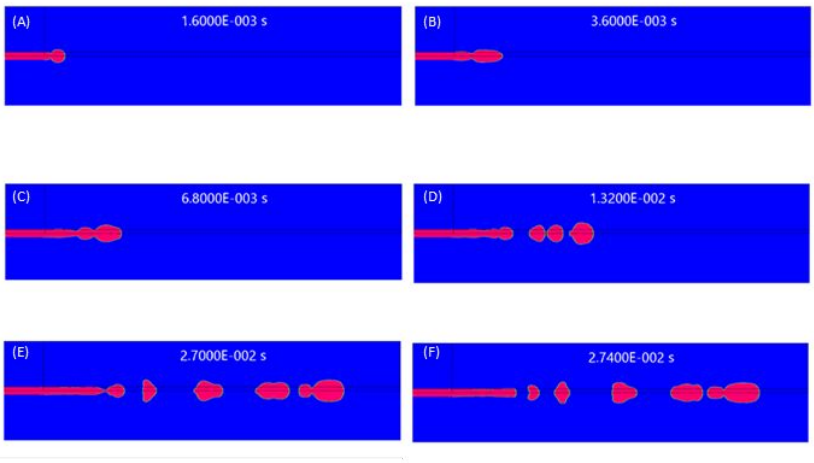


Figure 17- EHD Jetting at a flow rate of 1m/s and applied voltage of 4KV. A) t = 1.6s, droplet deforms into oblate shape (B) t = 3.6ms, droplet deforms into prolate shape (C) 6.8ms, (D) 13.2ms, droplet detaches (E) 27.0ms, the pinch point before droplet detachment is captured here and (F) 27.4ms, further droplet detachment and droplet advances towards the target wall.

From Figure 17, it was observed that at lower electric field strengths and higher flow rates, the liquid exhibits the dipping mode. A result consistent to reports from Wu et al [33] where a dipping mode was generated at lower electric field strength, as shown in Figure 13. The jet gradually develops into an oblate shape after 1.6ms and into a prolate shape after 3.6ms as the surface tension is overcome by the pull of the electric field. As the stretching continues, more deformation is observed and at 8.8ms, the first droplet detaches from the jet. At various instances, multiple jetting was observed at the jets also coalesce and further split. See supplementary material 2 for the movie of this droplet formation. Lopez-Herrera and his colleagues[43] also concluded in their work that the shape a deformed droplet assumes (either oblate or prolate) is dependent on the ratio of the droplet radius to the Debye length (which is a measure of the electrostatic effect on the charged droplet). As the electric field overcomes the surface tension of the fluid, the droplet deforms from an oblate shape into a prolate shape.

## 4. Conclusions

We present a general method capable of simulating a wide variety of electrohydrodynamic flows. The method is general in the sense that it can account for a wide variety of geometric configurations, combinations of fluid properties and an equally broad range of parameters, like liquid and gas flow rates, voltages, ambient atmosphere conditions and pressure, etc. Also, the jet/droplet diameter can either be smaller or comparably the same as the capillary diameter depending on the flow rate and the electric field strength, just as reported by Anna et al [44].

The method is based on the premise that the coupling of the two fields (flow and electric) is strongly bi-directional. This interplay gives rise to high levels of complexity but also allows for great control over the conditions at play. Therefore, this interaction of the electric field with the fluid, as studied and analysed numerically in this work, offers great potential for control of interesting and useful emerging features, such as specific size-controlled microbubbles.

## 5. Acknowledgements

The authors would like to acknowledge the financial and technical support provided by the ESI Group in association with the use of its CFD-ACE+ software package throughout this research.

## 6. References


(1) Castellanos, A. *Electrohydrodynamics*; Springer, 2014; Vol. 380.

(2) Saville, D. A. Electrohydrodynamics: The Taylor-Melcher Leaky Dielectric Model. *Annu. Rev. Fluid Mech.* **1997**, *29*, 27–64. https://doi.org/10.1146/annurev.fluid.29.1.27.

(3) Zhakin, A. I. Electrohydrodynamics. *Physics-Uspekhi* **2012**, *55* (5), 465–488. https://doi.org/10.3367/UFNe.0182.201205b.0495.

(4) Ramos, A.; Chen, C.-H. Electrohydrodynamic Stability. In *Electrokinetics and Electrohydrodynamics in Microsystems*; Springer Vienna, 2011; Vol. 530, pp 177–220. https://doi.org/10.1007/978-3-7091-0900-7_6.

(5) Zeng, J.; Sobek, D.; Korsmeyer, T. Electro-Hydrodynamic Modeling of Electrospray Ionization: CAD for a/Spl Mu/Fluidic Device-Mass Spectrometer Interface; IEEE; Vol. 2, pp 1275–1278.

(6) Baji, A.; Mai, Y. W.; Wong, S. C.; Abtahi, M.; Chen, P. Electrospinning of Polymer Nanofibers: Effects on Oriented Morphology, Structures and Tensile Properties. *Compos. Sci. Technol.* **2010**, *70* (5), 703–718. https://doi.org/10.1016/j.compscitech.2010.01.010.

(7) Rafiel, S.; Maghsoodloo, S.; Noroozi, B.; Mottaghitalab, V.; Haghi, A. K. Mathematical Modeling In Electrospinning Process of Nanofibers: A Detailed Review. *Cellul. Chem. Technol.* **2013**, *47* (5–6), 323–338.

(8) Garg, K.; Bowlin, G. L. Electrospinning Jets and Nanofibrous Structures. *Biomicrofluidics* **2011**, *5* (1), 13403.

(9) Wang, X.; Lin, T. *Needleless Electrospinning of Nanofibers: Technology and Applications*; CRC Press, 2013.

(10) Haghi, A. K.; Akbari, M. Trends in Electrospinning of Natural Nanofibers. *Phys. status solidi* **2007**, *204* (6), 1830–1834. https://doi.org/10.1002/pssa.200675301.

(11) Collins, R. T.; Harris, M. T.; Basaran, O. A. Breakup of Electrified Jets. *J. Fluid Mech.* **2007**, *588*, 75–129. https://doi.org/10.1017/S0022112007007409.

(12) Yarin, A. L.; Koombhongse, S.; Reneker, D. H. Taylor Cone and Jetting from Liquid Droplets in Electrospinning of Nanofibers. *J. Appl. Phys.* **2001**, *90* (9), 4836–4846.

(13) Reneker, D. H.; Yarin, A. L.; Fong, H.; Koombhongse, S. Bending Instability of Electrically Charged Liquid Jets of Polymer Solutions in Electrospinning. *J. Appl. Phys.* **2000**, *87* (9), 4531–4547.

(14) Reneker, D. H.; Chun, I. Nanometre Diameter Fibres of Polymer, Produced by Electrospinning. *Nanotechnology* **1996**, *7* (3), 216–223. https://doi.org/10.1088/0957-4484/7/3/009.

(15) Zeleny, J. Instability of Electrified Liquid Surfaces. *Phys. Rev.* **1917**, *10* (1), 1–6. https://doi.org/10.1103/PhysRev.10.1.

(16) Taylor, G. Disintegration of Water Drops in an Electric Field. *Proc. R. Soc. A Math. Phys. Eng. Sci.* **1964**, *280* (1382), 383–397. https://doi.org/10.1098/rspa.1964.0151.

(17) Ajayi, O. O. A Note on Taylor's Electrohydrodynamic Theory; The Royal Society; Vol. 364, pp 499–507.

(18) Taylor, G. Electrically Driven Jets. *Proc. R. Soc. London. A. Math. Phys. Sci.* **1969**, *313* (1515), 453–

475.

(19) Melcher, J. R.; Taylor, G. I. Electrohydrodynamics: A Review of the Role of Interfacial Shear Stresses. *Annu. Rev. Fluid Mech.* **1969**, *1* (1), 111–146.

(20) Hartman, R. P. A.; Brunner, D. J.; Camelot, D. M. A.; Marijnissen, J. C. M.; Scarlett, B. Electrohydrodynamic Atomization in the Cone-Jet Mode Physical Modeling of the Liquid Cone and Jet. *J. Aerosol Sci.* **1999**, *30* (7), 823–849. https://doi.org/10.1016/S0021-8502(99)00033-6.

(21) Hartman, R. P. A.; Brunner, D. J.; Camelot, D. M. A.; Marijnissen, J. C. M.; Scarlett, B. Electrohydrodynamic Atomization in the Cone-Jet Mode Physical Modeling of the Liquid Cone and Jet. *J. Aerosol Sci.* **1999**, *30* (7), 823–849. https://doi.org/10.1016/s0021-8502(99)00033-6.

(22) Yan, F.; Farouk, B.; Ko, F. Numerical Modeling of an Electrostatically Driven Liquid Meniscus in the Cone–jet Mode. *J. Aerosol Sci.* **2003**, *34* (1), 99–116. https://doi.org/10.1016/S0021-8502(02)00146-5.

(23) Lastow, O.; Balachandran, W. Numerical Simulation of Electrohydrodynamic (EHD) Atomization. *J. Electrostat.* **2006**, *64* (12), 850–859.

(24) Xu, J. H.; Li, S. W.; Chen, G. G.; Luo, G. S. Formation of Monodisperse Microbubbles in a Microfluidic Device. *AIChE J.* **2006**, *52* (6), 2254–2259. https://doi.org/10.1002/aic.10824.

(25) Gu, H.; Duits, M. H. G.; Mugele, F.; Gu, H.; Duits, M. H. G.; Mugele, F. Droplets Formation and Merging in Two-Phase Flow Microfluidics. *Int. J. Mol. Sci.* **2011**, *12* (4), 2572–2597. https://doi.org/10.3390/ijms12042572.

(26) Hayat, Z.; Abed, A. El; Hayat, Z.; El Abed, A. I. High-Throughput Optofluidic Acquisition of Microdroplets in Microfluidic Systems. *Micromachines* **2018**, *9* (4), 183. https://doi.org/10.3390/mi9040183.

(27) Sarkar, K.; Hoos, P.; Urias, A. Numerical Simulation of Formation and Distortion of Taylor Cones. *J. Nanotechnol. Eng. Med.* **2012**, *3* (4), 41001.

(28) Sen, A. K.; Darabi, J.; Knapp, D. R.; Liu, J. Modeling and Characterization of a Carbon Fiber Emitter for Electrospray Ionization. *J. Micromechanics Microengineering* **2006**, *16* (3), 620.

(29) Chen, C. Electrohydrodynamic Stability. **2011**, *220*, 177–220.

(30) Panofsky, W. K. H.; Phillips, M. *Classical Electricity and Magnetism*; Courier Corporation, 2005.

(31) Andrady, A. L. *Science and Technology of Polymer Nanofibers*; John Wiley & Sons, 2008.

(32) Fernández de La Mora, J. The Fluid Dynamics of Taylor Cones. *Annu. Rev. Fluid Mech.* **2007**, *39*, 217–243.

(33) Wu, X.; Oleschuk, R. D.; Cann, N. M. Characterization of Microstructured Fibre Emitters: In Pursuit of Improved Nano Electrospray Ionization Performance. *Analyst* **2012**, *137* (18), 4150–4161. https://doi.org/10.1039/c2an35249d.

(34) Jang, D. S.; Jetli, R.; Acharya, S. Comparison of the Piso, Simpler, and Simplec Algorithms for the Treatment of the Pressure-Velocity Coupling in Steady Flow Problems. *Numer. Heat Transf.* **1986**, *10* (3), 209–228. https://doi.org/10.1080/10407788608913517.

(35) Huang, M.; Wu, L.; Chen, B. Capturing Volume-of-Fluid Method Based on Unstructured Grids. *Numer. Heat Transf.* **2012**, *61* (5), 412–437. https://doi.org/10.1080/10407790.2012.672818.

(36) Teukolsky, S. A. Stability of the Iterated Crank-Nicholson Method in Numerical Relativity. *Phys. Rev. D* **2000**, *61* (8), 087501. https://doi.org/10.1103/PhysRevD.61.087501.

(37) Peterson; Richard. The Numerical Solution of Free-Surface Problems for Incompressible, Newtonian Fluids, The University of Leeds: The University of Leeda, 1999, Vol. Doctor of. https://doi.org/http://www.comp.leeds.ac.uk/research/pubs/theses/peterson.pdf.

(38) Hirt, C. W.; Nichols, B. D. Volume of Fluid (VoF) Method for the Dynamics of Free Boundaries. *J. Comput. Phys.* **1981**, *39* (1), 201–225. https://doi.org/10.1016/0021-9991(81)90145-5.

(39) Rider, W. J.; Kothe, D. B. Reconstructing Volume Tracking. *J. Comput. Phys.* **1998**, *141* (2), 112–152. https://doi.org/10.1006/JCPH.1998.5906.

(40) Karch, G. K.; Sadlo, F.; Meister, C.; Rauschenberger, P.; Eisenschmidt, K.; Weigand, B.; Ertl, T. Visualization of Piecewise Linear Interface Calculation; IEEE; pp 121–128.

(41) Hohman, M. M.; Shin, M.; Rutledge, G.; Brenner, M. P. Electrospinning and Electrically Forced Jets. I. Stability Theory. *Phys. Fluids* **2001**, *13* (8), 2201–2220.

(42) Kothandaraman, A.; Harker, A.; Ventikos, Y.; Edirisinghe, M.; Kothandaraman, A.; Harker, A.; Ventikos, Y.; Edirisinghe, M. Novel Preparation of Monodisperse Microbubbles by Integrating Oscillating Electric Fields with Microfluidics. *Micromachines* **2018**, *9* (10), 497. https://doi.org/10.3390/mi9100497.

(43) Lopez-Herrera, J. M.; Ganan-Calvo, A. M.; Popinet, S.; Herrada, M. A.; López-Herrera, J. M.; Gañán-Calvo, A. M. Electrokinetic Effects in the Breakup of Electrified Jets: A Volume-Of-Fluid Numerical Study. *Int. J. Multiph. Flow* **2015**, *71*, 14–22. https://doi.org/10.1016/j.ijmultiphaseflow.2014.12.005.

(44) Anna, S. L.; Bontoux, N.; Stone, H. A. Formation of Dispersions Using "Flow Focusing" in Microchannels. *Appl. Phys. Lett.* **2003**, *82* (3), 364–366. https://doi.org/10.1063/1.1537519.

TABLE OF CONTENT GRAPHIC